A Visual Feedback-based Time-Optimal Motion Policy for Capturing an Unpredictable Evader

David Jacobo[a], Ubaldo Ruiz[a], Rafael Murrieta-Cid[a], Hector M. Becerra[a*] and Jose Luis Marroquin[a**]

[a]*Centro de Investigación en Matemáticas, Guanajuato México (e-mails:{jguillen; ubaldo; murrieta; hector.becerra; jlm}@cimat.mx).*

In this paper, we address the pursuit/evasion problem of capturing an unpredictable omnidirectional evader using a Differential Drive Robot (DDR) in an obstacle-free environment. We present three main contributions: i) We provide a state feedback-based time-optimal motion policy for the DDR. The motion policy is based on a partition of the state space. One main contribution of this paper is to provide algebraic equations of the regions' boundaries of this partition in terms of the state space coordinates. ii) We estimate the state of the evader based on images using the 1D trifocal tensor. We propose a new formulation of the estimation of the evader's state relative to the pursuer. iii) We present a bound, for conventional cameras, over the pursuer's field of view that guarantees that, if the evader is initially visible, it will remain visible (inside the camera's view) regardless of its motion strategy, until the capture condition is achieved. We also present an implementation of the pursuer's motion policy, the estimation of the evader's state and also present simulation results of the pursuit/evasion game.

Keywords: Visual Feedback; Unpredictable Evader; Visual Servo-control; State Estimation; Optimal Control; Nonholonomic Constraints

1. Introduction

In Ruiz et al. (2013), we have considered the kinematic problem of capturing an omnidirectional evader using a Differential Drive Robot (DDR) in an obstacle-free environment. The DDR is faster than the evader, but it can only change its direction of motion at a maximum rate that is inversely proportional to its maximal translational speed (Balkcom & Mason (2002)). The game is over when the distance between the DDR and the evader is smaller than a critical value l. The DDR wants to minimize the capture time while the evader wants to maximize it.

In that work, we presented closed-form representations of the motion primitives and time-optimal strategies for each player in *open-loop*. We proposed a partition of the playing space into mutually disjoint regions where the strategies of the players are well established. This partition is represented as a graph which exhibits properties that guarantee global optimality. We also analyzed the decision problem of the game and presented the conditions defining the winner.

In this paper, we also consider the problem of capturing an omnidirectional evader using a DDR, but the players have different objectives. The DDR also wants to capture the evader in minimal time but now we assume that the evader *moves unpredictably*. The main motivation of this work is as following. Let us assume that the partition of the playing space is found. Let us also assume that the pursuer executes its time-optimal policy[1] but the evader moves unpredictably instead (i.e. its

---

[1]A policy is a rule that tells each player the control it has to apply at each time instant.

motion policy is unknown by the pursuer). If the pursuer executes its optimal policy in open-loop, i.e. $\gamma_p^*(t)$ (without evader state feedback), and the evader follows a suboptimal policy, i.e. $\gamma_e(t)$ then the pursuer might not be able to capture the evader. A simulation of this situation is included in Section 6.1. For this reason, in the case of an unpredictable evader, it is crucial for the pursuer to execute a state feedback-based motion policy. Note that in the case of an unpredictable evader the partition still provides a time-optimal pursuer motion policy, but the state $x(t)$ of the evader is needed by the pursuer to execute a state feedback-based time-optimal motion policy i.e. $\gamma_p^*(x(t))$. Thus, a novelty of this work is an approach that guarantees a pursuer's time-optimal policy based on visual feedback, for the case of an unpredictable evader.

In this work, we benefit from the work presented in Ruiz et al. (2013) and provide *three new* contributions. These contributions are:

i) We provide a state feedback-based motion policy for a DDR pursuer to capture an unpredictable evader. For a given state of the system, we provide a method to determine the pursuer's control that guarantees capture in minimal time. The main idea behind the approach is to obtain a closed-form polar representation of the singular surfaces (Başar & Olsder (1999); Isaacs (1965)) and the regions defined by them. In Ruiz et al. (2013) we use the Isaacs' methodology (Isaacs (1965)) and we presented a partition of the state space where the dividing surfaces were functions of the players' optimal controls and time. In this work, we provide algebraic equations for the surfaces that depend only on the state space coordinates. Note that the Isaacs' methodology provides the boundaries of such regions as a function of the players' optimal controls and time. But, that methodology *does not directly provide* algebraic equations of the regions' boundaries in terms of the state space coordinates. *In this paper one of our main contributions is to find these equations.*

ii) We estimate the state of the evader based on images taken by the pursuer using the 1D trifocal tensor (TT). The 1D TT has been used before for visual servoing purposes. In such problem the location of the robot is estimated in a global reference frame, which is defined by the robot's goal. In this paper, the goal of the robot is not defined by a specific location, but the robot's goal is to capture the evader, that is to move closer than a given distance from the evader. This requires defining the evader's location in a local reference frame defined by the pursuer, *which makes necessary a new formulation for state estimation compared with the one proposed in Becerra & Sagues (2013).* Furthermore, our approach does not require precise camera calibration and it is valid for different types of central cameras.

iii) We also present a bound over the pursuer's field of view that guarantees that, if the evader is initially visible, it will remain visible (inside the camera's view) regardless of its motion strategy, until the capture condition is achieved.

1.1   *Related Work*

The problem we consider in this paper is related to pursuit-evasion games. Many previous research exists in the area of pursuit and evasion, particularly in the area of dynamics and control in an environment without obstacles (Başar & Olsder (1999); Isaacs (1965)). The pursuit-evasion problem is often framed as a problem in noncooperative dynamic game theory (Başar & Olsder (1999); Shi (2014)).

A pursuit-evasion game can be defined in several ways. In one of them, one or more pursuers could be given the task of *finding* an evader (Hollinger et al. (2009); Isler et al. (2005)). To solve this problem, the pursuer(s) must sweep the environment so that the evader is not able to eventually sneak into an area that has already been explored. Deterministic (Guibas et al. (1999); Tovar & LaValle (2008)) and probabilistic algorithms (Chung (2008); Vidal et al. (2002)) have been proposed to solve this problem. A recent survey of this kind of problem is presented in Chung et al. (2011).

Alternatively, the pursuer(s) might have as a goal to capture the evader(s), that is, move to a contact configuration, or closer than a given distance. In the classical differential game, called the homicidal chauffeur problem (Isaacs (1965); Merz (1971)), a faster pursuer (w.r.t. the evader) has

as its objective to get closer than a given constant distance (the capture condition) from a slower but more agile evader in the Euclidean plane without obstacles.

Recent years have seen a growing interest in related problems within the robotics community. For instance, other related problem, which has been extensively studied, consists of *maintaining visibility of a moving evader* in an environment with obstacles (Bandyopadhyay et al. (2007); Bhattacharya & Hutchinson (2010); Efrat et al. (2003); Jung & Sukhatme (2002); LaValle et al. (1997); Murrieta et al. (2007); O'Kane (2008)). Game theory is proposed in LaValle et al. (1997) as a framework to formulate the tracking of a target, and an online algorithm is presented. In LaValle et al. (1997), an algorithm is presented that operates by maximizing the probability of future visibility of the evader.

In Efrat et al. (2003), the authors show how to efficiently (low-polynomial) compute an optimal reply path for the pursuer that counteracts *a given evader movement*. In O'Kane (2008), a robot has to track an unpredictable target with bounded speed. The robot's sensors are manipulated to record general information about the target's movements, and avoid that detailed information about the target's position be available if the robot's sensors are accessed by other agent that can damage the target.

Almost all existing work focuses on the 2-D version of the problem of maintaining visibility of an evader, but there are just some few works that deal with the 3-D version of it. In Bandyopadhyay et al. (2007), the authors present an online algorithm for 3-D target tracking among obstacles, using only local geometric information available to the robot's visual sensors.

The work presented in Bhattacharya & Hutchinson (2010) addresses the problem of maintaining visibility of the evader as a *game of degree* (i.e. the emphasis is over the optimization of a given criterion and not over the problem of deciding who is the winner). The pursuer and the evader are omnidirectional (holonomic) systems in an environment containing obstacles. In Bhattacharya & Hutchinson (2011), the problem of maintaining visibility of a moving evader is addressed as a *game of kind* (deciding which player wins). Again, both the pursuer and the evader are omnidirectional systems.

Others have studied an extended version of the problem involving multiple participants of each kind (evaders and pursuers) (Bhadauria & Isler (2011); Jung & Sukhatme (2002); Parker (2002)). For example, Parker (2002) developed a method that attempts to minimize the total time in which the evaders escape surveillance.

Maintaining visibility of a moving agent may be used in a variety of applications. For example, in Tekdas et al. (2010), the authors noticed the similarity between pursuit-evasion games and mobile-routing for networking. Applying this similarity, they proposed motion planning algorithms for robotic routers to maintain connectivity between a mobile user and a base station. That work also includes a proof-of-concept implementation. Similarly, in Stump et al. (2011) the authors consider the problem of deploying robots in formations that ensure network connectivity between a fixed base station and a set of independent agents wandering in the environment. The authors solved robots placements by finding mutually-visible configurations in a polygonal decomposition of the environment map.

Our problem is also related to the problem of finding optimal paths for nonholonomic robots (Balkcom & Mason (2002); Soueres & Laumond (1996); Wang et al. (2009)). These works belongs to the group of optimal control methods that are executed in open-loop. Such methods might benefit from results of the research on visual servoing of wheeled mobile robots (Becerra & Sagues (2013)). The work herein is a contribution to the efforts of executing an optimal policy in closed-loop, which is achieved for instance in Lopez-Nicolas et al. (2010). In that paper, the authors present a visual servo controller that effects optimal paths for a nonholonomic differential drive robot with field-of-view constraints. In the context of vision-based control, our work is related to the position-based visual servoing approach (Chaumette & Hutchinson (2006)), given that the proposed optimal policy relies on the estimation of the state of the system. However, in contrast to the classical position-based visual servoing approach in our proposed approach, the goal for the robot *is not to reach a place where a target image is observed*, but instead its objective is to

bring the evader to a specific locus of points called the usable part (Isaacs (1965)). Furthermore, the proposed state estimation using the 1D TT does not require precise camera calibration. In the literature, the 1D TT has been used to estimate the pose of a robot from visual data for visual servoing purposes (Becerra & Sagues (2013)). In this work a memoryless approach is used. Memoryless means that the pose parameters are estimated at each iteration directly from the current values of the tensor elements without using previous values of the estimated state.

2.   System Model

We can describe the kinematics of the game in a global coordinate system (refer to Fig. 1(a)), called in Isaacs (1965) the *realistic space*. The pose of the DDR is represented by (x_p, y_p, θ_p) and the position of the omnidirectional evader by (x_e, y_e), both at time t. The state of the system is denoted as $(x_p, y_p, \theta_p, x_e, y_e) \in \mathbb{R}^2 \times S^1 \times \mathbb{R}^2$.
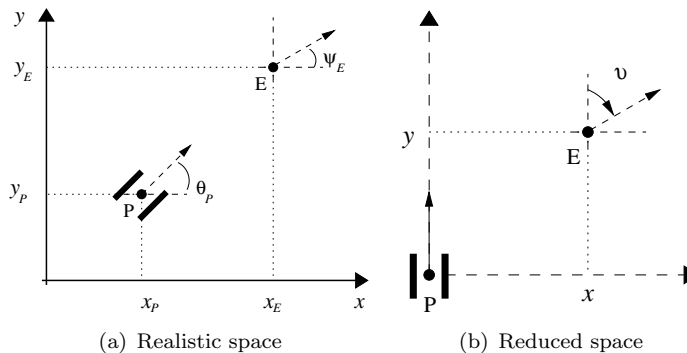

(a) Realistic space   (b) Reduced space

Figure 1. System models

2.1   *Reduced space*

To simplify the problem, we state the game in a coordinate system that is fixed to the DDR (see Fig. 1(b)), called in Isaacs (1965) the *reduced space*. In the reduced space all the orientations are measured with respect to the positive y-axis (DDR's heading). We denote the state of the system as $\mathbf{x}(t) = (x, y) \in \mathbb{R}^2$. Using the coordinate transformation given by

$$
\begin{aligned}
x &= (x_e - x_p) \sin \theta_p - (y_e - y_p) \cos \theta_p \\
y &= (x_e - x_p) \cos \theta_p + (y_e - y_p) \sin \theta_p \\
v_2 &= \theta_p - \psi_e
\end{aligned}
\tag{1}
$$

we obtain the following model of the kinematics in the reduced coordinate system (see Ruiz et al. (2013) for details).

$$
\begin{aligned}
\dot{x} &= \left(\frac{u_2 - u_1}{2b} \right) y + v_1 \sin v_2 \\
\dot{y} &= - \left(\frac{u_2 - u_1}{2b} \right) x - \left(\frac{u_1 + u_2}{2} \right) + v_1 \cos v_2
\end{aligned}
\tag{2}
$$

where $u_1, u_2 \in [-V_p^{\max}, V_p^{\max}]$ are the DDR's controls, and they correspond to the angular velocities of its wheels, u_1 is the angular velocity of the left wheel and u_2 of the right wheel. $v_1 \in [0, V_e^{\max}]$ and $v_2 \in [0, 2\pi)$ are the evader's controls associated to its speed and motion direction, respectively, in the reduced coordinate system. We can express this set of equations in the form $\dot{\mathbf{x}} = f(\mathbf{x}, u, v)$, where $u = (u_1, u_2) \in \widehat{U} = [-V_p^{\max}, V_p^{\max}] \times [-V_p^{\max}, V_p^{\max}]$ and $v = (v_1, v_2) \in \widehat{V} = [0, V_e^{\max}] \times [0, 2\pi)$.

4

Also one has the following inequality (3), which gives the maximum rate of rotation $\omega^{\max}$ for the pursuer, given a specified linear speed ν (Balkcom & Mason (2002); Ruiz et al. (2013)).

$$\omega = \frac{u_2 - u_1}{2b}$$
$$\nu = \frac{u_1 + u_2}{2} \tag{3}$$
$$|\omega^{\max}| \leq \frac{1}{b}(V_p^{\max} - |\nu|)$$

where ν is the DDR's translation speed and ω its angular speed.

We make use of the following definitions for the rest of the paper: $\rho_v = V_e^{\max}/V_p^{\max}$ is the ratio between the maximum translational speed of both players, and $\rho_d = b/l$ is the ratio of the distance between the center of the robot and the wheel location b and the capture distance l. Note that $l \geq b$, otherwise the capture distance would be located inside the robot.

## 3.   Partition Method for a State Feedback-based Motion Policy

In this section a partition of the state space into mutually disjoint regions is presented. This partition was found using Isaacs' methodology (Isaacs (1965)), which combines the theory of optimal control and differential games (Shi (2014)).

In Fig. 2(a), we have a graphical representation of the regions integrating the partition of the first quadrant of the reduced space. The frontiers between regions are called singular surfaces (Isaacs (1965)). In this partition, there are 4 singular surfaces (Ruiz et al. (2013)): universal surface (US, black bold line), transition surface (TS, red curve), the barrier surface (BS, magenta straight line) and dispersal surface (DS, orange line). If the pursuer applies its time-optimal motion policy the barrier cannot be crossed by the evader. The universal surface has the property that whenever the evader is located at US the time-optimal motion policy for the pursuer is to move in a straight line to capture it. The limit of the US is at $y_c = l/\rho_v$ (see Fig. 2(a)). The transition surface is the place where a control variable abruptly changes its value. A dispersal surface (DS) is defined in Isaacs (1965) as the locus of initial conditions along which the optimal strategy of one player or the optimal strategies of both players are not unique. At the DS, the choice of the control of one player must correspond to the choice of the control of the other player. In this problem, the DS corresponds to configurations where the pursuer's heading (orientation of the wheels) is perpendicular to the evader's location, and the DDR has the option to rotate either clockwise or counterclockwise to catch the evader. To avoid the selection problem, the instantaneous velocity vector of both players should be known, but in this problem, it is assumed that this information is not available. Therefore, a solution will be to employ an instantaneous mixed strategy (Isaacs (1965)), which means the randomizing of a player's decision in accordance with some probabilistic law until the system is no longer on the DS. The trajectories generated by the correct pair of controls will lead to the same optimal time-to-go. A more detailed description of each singular surface in the partition is presented in Ruiz et al. (2013). The partition also contains the terminal surface and the usable part (UP). The terminal surface is the set of points that represents an opportunity for the DDR to capture the evader (Isaacs (1965)). In this game it is a circle of radius l. The usable part (UP, black bold arc in Fig. 2(a)) is the portion of the space where the pursuer guarantees capture of the evader regardless of the choice of controls by the evader (Isaacs (1965)). The boundary of the usable part is the point BUP shown in Fig. 2(a).

The regions are equivalence classes under a relation given by the control, i.e. in the interior of each region the pursuer applies always its feedback-based time-optimal motion policy based on the location of the evader over the reduced space. This policy for the first quadrant is summarized in Table 1. In the remaining quadrants the pursuer time-optimal motion policy is analogous.
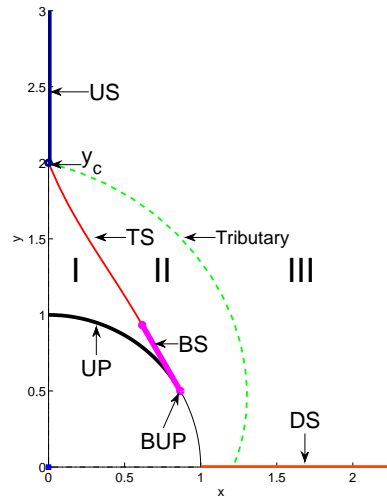
(a) Partition of the first quadrant and its singular surfaces
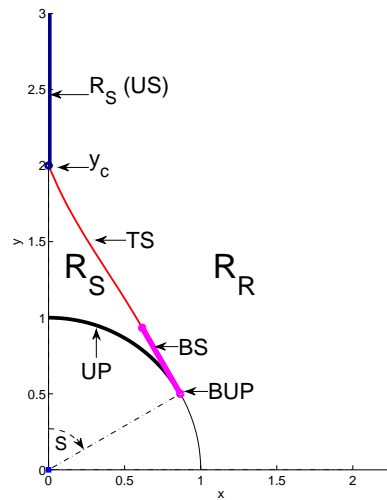
(b) Partition for pursuer's feedback motion policy

Figure 2. Partition of the first quadrant

Evader in the reduced space	u_1, u_2
US	$u_1 = +V_p^{\max}$, $u_2 = +V_p^{\max}$
I	$u_1 = +V_p^{\max}$, $u_2 = +V_p^{\max}$
II	$u_1 = +V_p^{\max}$, $u_2 = -V_p^{\max}$
III	$u_1 = +V_p^{\max}$, $u_2 = -V_p^{\max}$
DS	Randomized strategy

Table 1.   Pursuer's feedback-based time-optimal motion policy in quadrant 1.

If the evader is located in Region I then the DDR moves in a straight line in the realistic space to capture the evader. Region II corresponds to configurations in the realistic space where the DDR initially rotates in place, but it is not necessary to align completely the DDR's heading with the segment joining the positions of both players in order to capture the evader. Region III in the reduced space corresponds to configurations in the realistic space where the DDR also rotates in

place until it aligns its heading with the segment joining the players' position. The frontier between Region II and Region III is established by the tributary trajectory[2] (green dashed line) shown in Fig. 2(a).

From Table 1, we see that the US and Region I have associated the same optimal controls, and the same happens with regions II and III. Therefore, for the purposes of this work the partition shown in Fig. 2(a) might be simplified to one in which the US and Region I are merged and Region II and Region III are merged too. Furthermore, in this work it is assumed that no a priori information is available about the evader's motion policy and that it cannot be learned by the pursuer –i.e., the evader is totally unpredictable–. Therefore, the dispersal surface is also merged with region II and III. Hence, let $R_S=$ US $\cup$ Region I and $R_R=$ Region II $\cup$ Region III $\cup$ DS. Refer to Fig. 2(b). In the remaining of this paper, we shall provide algebraic equations for the singular surfaces in terms of the reduced space polar coordinates (r, ϕ). Such equations are used to identify the region, either R_S or R_R, of the reduced space partition where the evader belongs.

For convenience, a state (x, y) in the reduced space is represented in polar coordinates (r, ϕ); recall that the orientations are measured with respect to the positive y-axis.

$$r = \sqrt{x^2 + y^2}$$
$$\phi = \tan^{-1} \frac{x}{y} \tag{4}$$

To make this paper self-contained, we include an Appendix with four lemmas obtained in Ruiz et al. (2013), which are used in this work. Below, notation established in Ruiz et al. (2013) is used too. Specifically, $\tau = t_f - t$ denotes the retro-time, in which t_f is the termination time of the game. V_x and V_y denote the partial derivatives $\frac{\partial V}{\partial x}$ and $\frac{\partial V}{\partial y}$ of V, the value of the game. V_x and V_y can be interpreted as Lagrange multipliers. In Ruiz et al. (2013), the angle s denotes the angle measured from the positive y-axis to a point in the usable part, and S denotes a bound in s corresponding to the boundary of the usable part (BUP). Finally, λ is a constant value.

The idea behind the approach presented here is comparing the distance r from the origin of the reduced space to a given state (x, y) (evader's location over the reduced space) with the distance from the origin to the singular surfaces delimiting the regions R_S and R_R in the reduced space. In Fig. 2(b), one can observe that if $\phi = 0$ then the state does not belong to region R_R. Note that the US is easily characterized by $\phi = 0$ and $r \geq y_c$. One can also observe that Region R_R is bounded by the transition surface, the barrier and the terminal surface. Hence, if $\phi \in (0, \pi/2]$ we have three possible choices: one has to compare the distance r with (1) the distance from the origin to the transition surface or (2) the distance r_B from the origin to the barrier or (3) the distance l from the origin to the terminal surface.

In Fig. 2(b), one can also observe that the transition surface is bounded by the positive y-axis and the barrier. Once one finds the point (x, y) in the reduced space delimiting the transition surface and the barrier, it is straightforward to find the orientation of this point, by simply using $\phi = \tan^{-1}(\frac{x}{y})$. This is the upper bound orientation that has to be compared with the transition surface. In an analogous way, using the point of the barrier over the terminal surface (BUP) with respect to angle ϕ, one can find the upper bound orientation that has to be compared with the barrier. The remaining states have to be compared with the terminal surface.

In Lemma 1 the state (x, y) delimiting the transition surface and the barrier surface is established. In Lemma 2, an equation defining the transition surface in terms of the reduced space coordinates (r, ϕ) is found. In Lemma 3, the distance from the origin to the barrier r_B is found in terms of the reduced space coordinates (r, ϕ).

---

[2]A tributary trajectory is an optimal trajectory of the system in the reduced space that reach the (US).

Lemma 1: *The state (x, y) delimiting the TS and the BS is given by $x = -\frac{bV_e^{\max}\cos S}{V_p^{\max}} + l\sin S$ and $y = -\frac{bV_e^{\max}\cos^2 S}{V_p^{\max}\sin S} + \frac{b\cos S}{\sin S} + l\cos S$.*

Proof. From Lemma 5 in Appendix A, we know that the barrier starts (ends in retro-time) at $\tau = (b\cos S)/(V_p^{\max}\sin S)$, where $S = \cos^{-1}(V_e^{\max}/V_p^{\max})$. The trajectory of the barrier in the first quadrant is given by

$$
\begin{aligned}
x(\tau) &= -\tau V_e^{\max}\sin S + l\sin S \\
y(\tau) &= -\tau V_e^{\max}\cos S + V_p^{\max}\tau + l\cos S
\end{aligned}
\tag{5}
$$

Hence, we have that the state delimiting the TS and BS is given by

$$
\begin{aligned}
x &= -\frac{bV_e^{\max}\cos S}{V_p^{\max}} + l\sin S \\
y &= -\frac{bV_e^{\max}\cos^2 S}{V_p^{\max}\sin S} + \frac{b\cos S}{\sin S} + l\cos S
\end{aligned}
\tag{6}
$$

The orientation ϕ_{TS} of this state is given by $\phi_{TS} = \tan^{-1}\frac{x}{y}$. The result follows. $\qquad\square$

In contradistinction to the US and the BS, the TS is not a trajectory traveled by the system in the reduced space, and it cannot be directly obtained from the backward integration of the motion equations. In this work, we construct an implicit representation in polar coordinates (r, ϕ) using the expressions from the player's optimal controls. In the first quadrant, the TS represents the locus of points where the DDR switches one of its controls, in particular from Lemma 6 in Appendix A, we found that u_2^* switches from the value $V_p^{\max}$ to $-V_p^{\max}$. The expression defining the control u_2^* at the moment of the switch characterizes the conditions that must satisfy the points (x, y) in the reduced space. In this work, the control expressions give us a relation between the polar coordinates (r, ϕ) of the points (x, y) and the values of the adjoint variables V_x and V_y at the moment of the switch (see Lemma 7 in Appendix A). Using this characterization of the TS we can determine if a point (r, ϕ) belongs to the surface or if it is above or below it.

Lemma 2: *If the left term of Eq. (7), presented below is greater than zero then the state is above the transition surface and it belongs to Region R_R.*

$$
\begin{aligned}
&r^4\sin^2\phi\cos^2\phi + r^4\sin^4\phi + 2br^3\sin^3\phi \\
&+ b^2r^2\sin^2\phi - \frac{V_e^{\max 2}}{V_p^{\max 2}}b^2r^2\cos^2\phi + 2\frac{V_e^{\max}}{V_p^{\max}}blr^2\sin\phi\cos\phi \\
&+ 2\frac{V_e^{\max}}{V_p^{\max}}b^2lr\cos\phi - l^2r^2\sin^2\phi - 2bl^2r\sin\phi - l^2b^2 = 0
\end{aligned}
\tag{7}
$$

Proof. In the first quadrant, the TS represents the locus of points where the DDR switches one of its controls, from Lemma 6 in Appendix A, we know that for the first quadrant, u_2^* switches first, therefore along the TS the expression defining the control u_2^* is given by

$$
yV_x - xV_y - bV_y = 0
\tag{8}
$$

where (x, y) are the coordinates of the system in the reduced space when the DDR switches controls. In Lemma 7 in Appendix A, from the backward integration of the adjoint equation starting at the UP, we find that $V_x = \lambda\sin s$ and $V_y = \lambda\cos s$ just before the switch. Therefore Eq. (8) takes the

form

$$y\lambda \sin s - x\lambda \cos s - b\lambda \cos s = 0 \tag{9}$$

where s is the angle of the point in UP, whose optimal trajectory from the UP to the TS intersects the point (x, y). Doing some algebraic manipulation of Eq. (9), we find that

$$\tan s = \frac{x + b}{y} \tag{10}$$

From Lemma 8 in Appendix A, we know that all retro-time straight line trajectories in the reduced space that have an initial orientation $s \in (\tan^{-1}(\rho_v \rho_d), \cos^{-1}(\rho_v)]$ in the UP, reach the TS. The straight line trajectories in the reduced space starting at UP are given by

$$
\begin{aligned}
x(\tau) &= -\tau V_e^{\max} \sin S + l \sin S \\
y(\tau) &= -\tau V_e^{\max} \cos S + V_p^{\max}\tau + l \cos S
\end{aligned}
\tag{11}
$$

From Lemma 6 in Appendix A, we know that the DDR switches u_2^* at $\tau = (b \cos s)/(V_p^{\max} \sin s)$. Thus, the x-coordinates along the TS are given by

$$x = \frac{-bV_e^{\max}\cos s}{V_p^{\max}} + l \sin s \tag{12}$$

Recalling that $\sin(\arctan(x)) = \frac{x}{\sqrt{1+x^2}}$ and $\cos(\arctan(x)) = \frac{1}{\sqrt{1+x^2}}$, and substituting Eq. (10) into Eq. (12), we have that

$$x = \frac{-b\frac{V_e^{\max}}{V_p^{\max}} + l\left(\frac{x+b}{y}\right)}{\sqrt{1 + \left(\frac{x+b}{y}\right)^2}} \tag{13}$$

Doing some algebraic manipulation of the expression above, and recalling that $x = r \sin \phi$ and $y = r \cos \phi$, we find that

$$
\begin{aligned}
&r^4 \sin^2 \phi \cos^2 \phi + r^4 \sin^4 \phi + 2br^3 \sin^3 \phi \\
&+ b^2 r^2 \sin^2 \phi - \frac{V_e^{\max 2}}{V_p^{\max 2}} b^2 r^2 \cos^2 \phi + 2\frac{V_e^{\max}}{V_p^{\max}} blr^2 \sin \phi \cos \phi \\
&+ 2\frac{V_e^{\max}}{V_p^{\max}} b^2 lr \cos \phi - l^2 r^2 \sin^2 \phi - 2bl^2 r \sin \phi - l^2 b^2 = 0
\end{aligned}
\tag{14}
$$

The result follows. $\qquad\square$

In the next lemma an equation establishing the distance r_B is found. Using this equation, one can compare the distance r and the distance r_B to identify if the evader's state belongs to region R_R.

Lemma 3: *The distance r_B from the origin of the reduced space to a point $(r, \phi) \in BS$ is given by Eq. (15):*

$$r_B = \frac{V_p^{\max} l \sin S}{V_p^{\max} \sin \phi - V_e^{\max} \sin(\phi - S)} \tag{15}$$

Proof. We know that the barrier in the first quadrant is given by

$$x = -\tau V_e^{\max} \sin S + l \sin S \tag{16}$$

$$y = -\tau V_e^{\max} \cos S + \tau V_p^{\max} + l \cos S \tag{17}$$

where $S = \cos^{-1}(V_e^{\max}/V_p^{\max})$ From Eq. (16), we have that

$$\tau = \frac{l \sin S - x}{V_e^{\max} \sin S} \tag{18}$$

and from Eq. (17), we have that

$$\tau = \frac{l \sin S - y}{V_e^{\max} \sin S - V_p^{\max}} \tag{19}$$

Equating Eq. (18) and Eq. (19), we obtain

$$-V_p^{\max} l \sin S + x V_p^{\max} = -V_e^{\max} y \sin S + V_e^{\max} x \cos S \tag{20}$$

Substituting $x = r \sin \phi$ and $y = r \cos \phi$ in the equation above, and applying some trigonometric identities, we have that

$$r_B = \frac{V_p^{\max} l \sin S}{V_p^{\max} \sin \phi - V_e^{\max} \sin(\phi - S)} \tag{21}$$

The result follows. □

The next theorem establishes which are the controls that the pursuer must apply to capture the evader in minimum time according to the region in the reduced space where the evader is located.

Theorem 1: *The optimal controls for the pursuer are $u_1 = +V_p^{\max}$, $u_2 = -V_p^{\max}$ if*

$$(r, \phi) \in R_R \text{ or equivalently } \begin{cases} \phi \in (0, \phi_{TS}) \text{ and } Eq.(7) > 0 \text{ or} \\ \phi \in [\phi_{TS}, \phi_B] \text{ and } r > r_B \text{ or} \\ \phi \in (\phi_B, \frac{\pi}{2}] \text{ and } r \geq l \end{cases} \tag{22}$$

Otherwise the optimal controls are $u_1 = +V_p^{\max}$, $u_2 = +V_p^{\max}$, except when $r < l$ establishing that the evader capture has been achieved.

Proof. The transition surface (TS) is delimited in ϕ by the interval $(0, \phi_{TS})$. By Lemma 1, $\phi = \phi_{TS}$ represents an upper bound of the transition surface with respect to ϕ. By Lemma 2, if the left term of Eq. (7) is greater than zero then the evader state (r, ϕ) is above the transition surface. Hence, if the left term of Eq. (7) > 0 and $\phi \in (0, \phi_{TS})$ then the evader state (r, ϕ) belongs to region R_R. The barrier (BS) is delimited in ϕ by the interval $[\phi_{TS}, \phi_B]$. By Lemma 3, the distance from the origin of the reduced space to a point in the barrier is given by Eq. (15). By Lemma 5 in Appendix A, $\phi_B = \cos^{-1}(V_e^{\max}/V_p^{\max})$ (Ruiz et al. (2013)). Therefore, if $r > r_B$ and $\phi \in [\phi_{TS}, \phi_B]$ then the evader state (r, ϕ) belongs to region R_R. Finally, the portion of the terminal surface corresponding to a boundary of region R_R is delimited by the interval $(\phi_B, \frac{\pi}{2})$. Hence, if $r \geq l$ and $\phi \in (\phi_B, \frac{\pi}{2})$ then the evader state (r, ϕ) belongs to region R_R. This completes the proof. □

4.   State Determination Using Visual Information and the 1D Trifocal Tensor

In this section, we define an adequate framework to retrieve from the 1D Trifocal Tensor (TT) the relative geometry between a pursuer carrying a camera and an omnidirectional evader that can be seen by the pursuer's camera along the game. The 1D TT is a geometric constraint that relates the visual information from three views of the same scene, with the corresponding camera positions and orientations, in the frame of planar motion.

In general, having two images of an adequate pattern of 3D points, which are captured from two collinear camera locations in a plane where the relative distance between them is known, it is possible to estimate the location and orientation of the third camera in the same plane from the image of the pattern in this camera through the 1D TT relating the three images.

First, we present the general framework of the 1D TT and next, we formulate the particular case for the pursuer-evasion game. The 1D TT has two main advantages that make it interesting for robotics applications: 1) the 1D TT can be estimated without a precise camera calibration, and 2) the estimation method based on the 1D TT is similar for conventional cameras and for central catadioptric systems assuming that all of them approximately obey the generic central camera model (Geyer & Daniilidis (2000)).
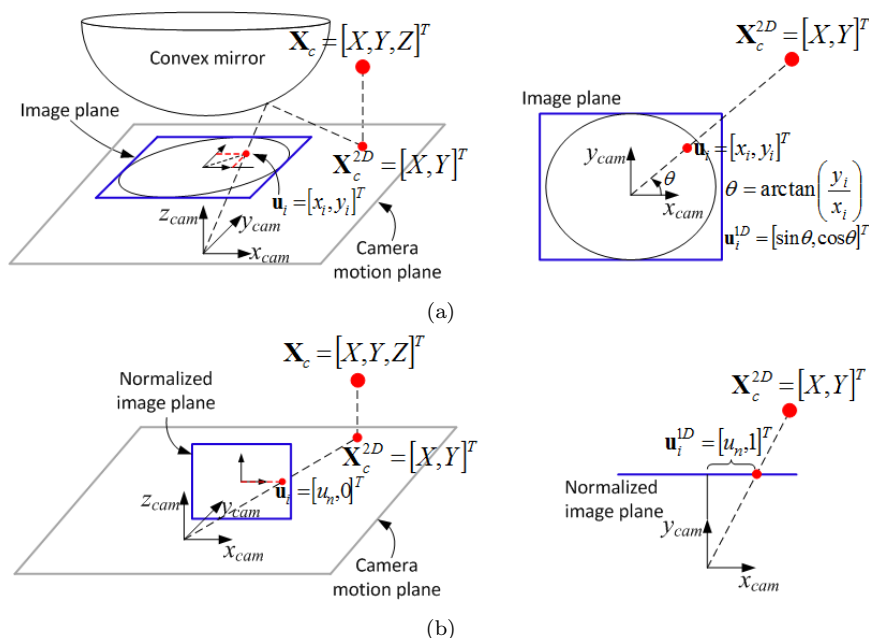

Figure 3.   Formulation to obtain bearing measurements as a one-dimensional projection valid for different types of central cameras. (a) Omnidirectional camera looking upward. (b) Conventional camera looking forward. The right panels depict bird-eye's views of the cameras

Under the 1D projective formulation shown in Fig. 3, let us consider three 1D projective points in homogeneous coordinates $\mathbf{u} = [u_1, u_2]^T$, $\mathbf{v} = [v_1, v_2]^T$ and $\mathbf{w} = [w_1, w_2]^T$, which are bearing measurements that represent the projections of a point $\mathbf{X}_c^{2D}$ from three different camera locations. We assume that the camera locations are constrained to the x-y plane. For an omnidirectional camera, each one of the 1D projective points is given as $\mathbf{u}_i^{1D} = [\sin\theta, \cos\theta]^T$ (see the right panel of Fig. 3(a)). For a conventional camera, the 1D projective points are given as $\mathbf{u}_i = [u_n, 0]^T$, where u_n is the x-coordinate of the normalized image point (see the right panel of Fig. 3(b)). u_n can be obtained from the image x-coordinate u in pixels as follows:

$$u_n = \frac{1}{f_x}(u - u_0) \tag{23}$$

11

where f_x is the focal length of the camera in terms of pixel dimensions in the x-direction and u_0 is the x-coordinate of the principal point in pixels. Both parameters f_x and u_0 can be estimated as proposed in Faugeras et al. (2000) from 3 images obtained from 3 different camera locations. This may be done off-line in the initialization phase of the procedure (see Algorithm 1).

The TT establishes a relation between the homogeneous image coordinates $\mathbf{u}, \mathbf{v}, \mathbf{w}$ and the corresponding camera locations (Becerra & Sagues (2013); Guerrero et al. (2008)). Consider a point $\mathbf{X}$ in a 2D space given in homogeneous coordinates as shown in Fig. 4. Three camera locations are represented with a global reference frame attached to the second view, and the point $\mathbf{X}$ is expressed in that frame. For each view, the line parallel to the local x-axis represents the bird-eye's view of the image plane if the camera is conventional and the circle represents the bird-eye's view of the image plane if the camera is omnidirectional. The 1D projective formulation of the point $\mathbf{X}$ for each view results in the bearing observations $\mathbf{u} = [u_1, u_2]^T$, $\mathbf{v} = [v_1, v_2]^T$ and $\mathbf{w} = [w_1, w_2]^T$, obtained as explained in Fig. 3 for different types of cameras.
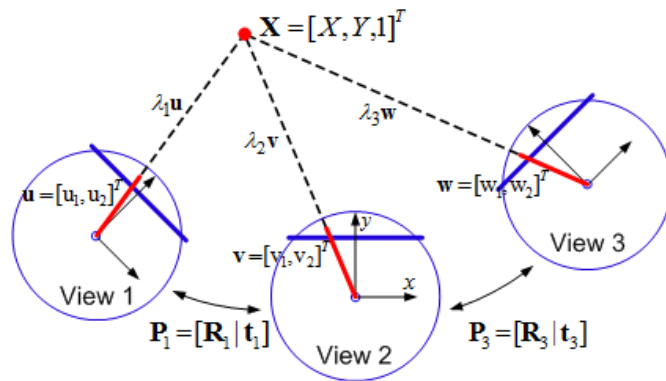

Figure 4. Bearing observations $\mathbf{u}$, $\mathbf{v}$, $\mathbf{w}$ in the framework of the 1D TT

Note that, the position vector of the point $\mathbf{X}$ from each local reference frame can be expressed as $\lambda_1 \mathbf{u}$, $\lambda_2 \mathbf{v}$ and $\lambda_3 \mathbf{w}$, respectively, where λ_1, λ_2 and λ_3 are scale factors related to the corresponding magnitude of the position vectors. The following trifocal constraint relates the visual data $\mathbf{u}$, $\mathbf{v}$ and $\mathbf{w}$:

$$\sum_{i=1}^{2}\sum_{j=1}^{2}\sum_{k=1}^{2} T_{ijk} u_i v_j w_k = 0 \tag{24}$$

where the tensor elements T_{ijk} are given by:

$$\mathbf{T}_{ijk} = \begin{bmatrix} T_{111} \\ T_{112} \\ T_{121} \\ T_{122} \\ T_{211} \\ T_{212} \\ T_{221} \\ T_{222} \end{bmatrix} = \frac{1}{\alpha} \begin{bmatrix} t_{y_1}s\phi_3 - t_{y_3}s\phi_1 \\ t_{y_1}c\phi_3 + t_{x_3}s\phi_1 \\ t_{y_3}c\phi_1 - t_{y_1}c\phi_3 \\ t_{y_1}s\phi_3 - t_{x_3}c\phi_1 \\ -t_{y_3}c\phi_1 - t_{x_1}s\phi_3 \\ t_{x_3}c\phi_1 - t_{x_1}c\phi_3 \\ t_{x_1}c\phi_3 - t_{y_3}s\phi_1 \\ t_{x_3}s\phi_1 - t_{x_1}s\phi_3 \end{bmatrix} \tag{25}$$

where α is the scale factor introduced by the estimation of the 1D TT from visual data and $t_{x_i} = -x_i c\phi_i - y_i s\phi_i$ and $t_{y_i} = x_i s\phi_i - y_i c\phi_i$ for $i = 1, 3$. Notice that t_{x_i} and t_{y_i} are the relative positions between cameras by defining local reference frames in each camera as depicted in Fig. 5.
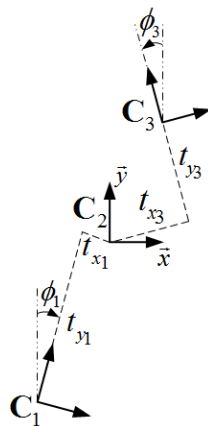
Figure 5. Relative locations from local reference frames $\mathbf{C}_1$ and $\mathbf{C}_3$ to $\mathbf{C}_2$

The proposed strategy for determining the relative location and pose between the pursuer and evader entails solving the expression in Eq. (24). Since Eq. (24) is a homogeneous equation, the eight elements of the 1D TT can only be estimated up to a scale factor. Thus, the 1D TT has seven degrees of freedom and we have to stack at least seven Eqs. (24) and solve the resultant linear system of equations. Therefore, in general, seven triplets of image point correspondences are needed to estimate the 1D TT. Note that in general this system of linear equations does not have full rank, so that one must use methods like SVD for solving it.

Our goal is to estimate the evader's position in the reduced space (a local reference frame defined over the pursuer's location; see Fig. 1(b)) using the 1D TT. To do so, it is necessary to have, in addition to the image obtained by the pursuer at the current location, –which in what follows will correspond to the image taken from the camera $\mathbf{C}_3$– two additional images taken as part of the initialization procedure; i.e., images taken from camera positions $\mathbf{C}_1$ and $\mathbf{C}_2$. These auxiliary locations are determined with respect to the evader: a first image is taken at a distance d_e directly in front of the evader. Then, the pursuer's camera moves backward and a second image is taken at a distance d_i from $\mathbf{C}_2$. Note that these 2 images are taken only once and do not change.

In the local reference frame $\mathbf{C}_2$, which is attached to the evader and hence moves and rotates together with it, the position and orientation of camera $\mathbf{C}_1$ are $\phi_1 = t_{x_1} = 0$; $t_{y_1} = d_i$, and the evader's position is $(0, d_e)$, see Fig. 6.

To obtain the position (x, y) of the evader in the local reference frame attached to $\mathbf{C}_3$ –i.e., its position in the reduced space of the pursuer– one uses first the 1D TT to obtain the pose parameters of the current pursuer's location $\mathbf{C}_3$ with respect to $\mathbf{C}_2$, measured with respect to a local reference frame attached to $\mathbf{C}_3$, i.e. t_{x_3}, t_{y_3} and ϕ_3 in Fig. 6.

The tensor elements in Eq. (25) now become

$$\begin{bmatrix} T_{111} \\ T_{112} \\ T_{121} \\ T_{122} \\ T_{211} \\ T_{212} \\ T_{221} \\ T_{222} \end{bmatrix} = \frac{1}{\alpha} \begin{bmatrix} d_i \mathrm{s}\phi_3 \\ d_i \mathrm{c}\phi_3 \\ t_{y_3} - d_i \mathrm{c}\phi_3 \\ d_i \mathrm{s}\phi_3 - t_{x_3} \\ -t_{y_3} \\ t_{x_3} \\ 0 \\ 0 \end{bmatrix} \tag{26}$$

The pose parameters of the current pursuer's location $\mathbf{C}_3$ measured from a local reference frame attached to $\mathbf{C}_3$ are given by:
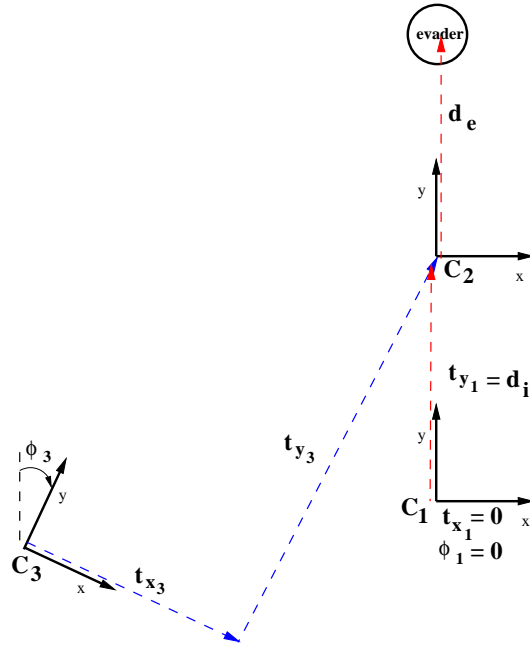
13

Figure 6.   Geometric configuration for estimation of the relative locations between evader and pursuer in the framework of the 1D TT

$$\phi_3 = \tan^{-1}\left(T_{111}/T_{112}\right) \tag{27}$$
$$t_{x_3} = \alpha T_{212}$$
$$t_{y_3} = -\alpha T_{211}$$

where the overall scale factor can be computed as:

$$\alpha = \left(d_i \cos\phi_3\right)/T_{112} \tag{28}$$

The evader's position in the local reference frame $\mathbf{C}_3$ (i.e. the evader's coordinates in the reduced space of the pursuer) are then:

$$x = t_{x_3} - \sin\phi_3 d_e$$
$$y = t_{y_3} + \cos\phi_3 d_e \tag{29}$$

Which may be transformed to polar coordinates using Eq. (4), and then to determine the regions of the state space partition of Fig. 2(b) where the system is located and hence, the optimal control policy for the pursuer according to Theorem 1.

In the case of conventional cameras, the parameters u_0 and f_x that appear in Eq. (23) must be estimated as part of the initialization procedure. If the procedure of Faugeras et al. (2000) is used the only thing one needs, in addition to the images taken from the camera locations $\mathbf{C}_1$ and $\mathbf{C}_2$ is a third image taken from an arbitrary location, provided that this camera's orientation is different from the ones of $\mathbf{C}_1$ and $\mathbf{C}_2$. In the case of omnidirectional cameras this step is not needed.

A necessary condition for the good estimation of the 1D TT is that at least seven of the used image points have different bearings, otherwise, the estimation is unstable and the resultant tensor is not a valid constraint. Since the 1D TT is estimated from image points detected over the body

of the evader, it can be ensured to have different bearing measurements by using an appropriate visual pattern over the evader.

It is worth noting that during the pursuer motion, it might happen (although with a very low probability) that the current image becomes the same as one of the auxiliary images. This situation is a degenerated case of the 1D TT formalism and the state estimation will fail. This case can be detected by using an error value defined in Guerrero et al. (2008), which is the average difference between the observed coordinates and the coordinates estimated from transfer of points using the trifocal tensor.

Algorithm 1 summarizes the whole proposed time-optimal motion policy based on state estimation from images, including a strategy for dealing with degenerated cases where two images become the same. Notice that if a degenerated situation happens then the current position of the evader is directly in front of the pursuer, which means that the evader is at the US in the reduced space. Therefore, the controls corresponding to the US must be applied.

> **Initialization**:
> 1. Take the images I_1 and I_2 associated to $\mathbf{C}_1$ and $\mathbf{C}_2$;
> 2. Measure the distances d_i and d_e;
> 3. For conventional cameras, estimate the camera parameters u_0 and f_x, using images I_1, I_2 and a third image I_3 taken from a different location and orientation using the method of Faugeras et al. (2000).
> **Input**: Image I_3 associated to $\mathbf{C}_3$, d_i and d_e;
> **Output**: Pursuer's optimal controls u_1 and u_2;
> 4. Automatic matching of $n > 7$ image points from I_1, I_2 and I_3;
> 5. 1D projective formulation of the n corresponding image points to have $\mathbf{u}^m$, $\mathbf{v}^m$ and $\mathbf{w}^m$ for $m = 1, ..., n$;
> **while** capture $\neq$ true **do**
>   6. Estimate the 1D TT through an SVD approach;
>   **if** $E >$ threshold (E as defined in Guerrero et al. (2008)) **then**
>   7. Apply $u_1 = +V_p^{\max}$ and $u_2 = +V_p^{\max}$;
>   **else**
>   8. Compute r and ϕ from the estimated evader position given by Eq. (4);
>   9. Apply the pursuer's optimal controls u_1 and u_2 according to Theorem 1;
>   **end if**
>   10. Track the corresponding image points on the new I_3 and formulate $\mathbf{w}^m$ for $m = 1, ..., n$;
> **end while**

Algorithm 1: Algorithm for the time-optimal motion policy based on state estimation from images.

5. A bound for the angle delimiting the field of view of the pursuer and other sensing issues

In this section, we will show that if the pursuer's sensor is a pinhole camera with field of view (FOV) that includes the boundary of the usable part (BUP), then if the evader is visible at the beginning of the game and the pursuer follows the optimal feedback policy then the evader will remain visible until the capture is achieved regardless of the evader's motion strategy.

Without loss of generality assume that the evader is in the first quadrant of the reduced space (the proofs for the remaining quadrants are analogous), and assume that the pursuer's FOV is delimited by a line in the reduced space with angle ϕ_v (measured from the positive y-axis). The angle defining the boundary of the usable part (BUP) is $S = \cos^{-1}(\rho_v)$ (Ruiz et al. (2013)) and assume that $S < \phi_v$ (see Fig. 7). We then have the following.

Theorem 2: *If the evader is in position (r_0, ϕ_0) in the reduced space at the beginning of the game with $\phi_0 < \phi_v$ and $S < \phi_v$ then, if the pursuer applies its time-optimal feedback policy the evader's position (r, ϕ) will satisfy $\phi < \phi_v$ at all times until the capture is achieved regardless of the evader's motion strategy.*
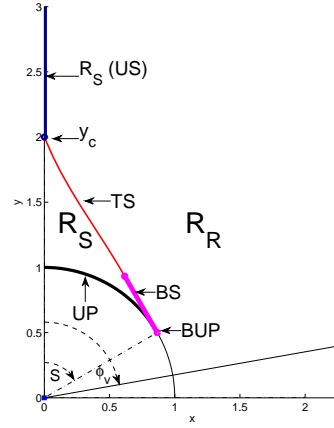
Figure 7. Angle S and angle ϕ_v

To prove this theorem, we need the following lemma.

Lemma 4: *If the evader is at position (L, ϕ) in region R_R with $L \geq l$ and the pursuer applies its time-optimal feedback policy then $\dot{\phi} < 0$ regardless of the evader's motion strategy.*

Proof. The Cartesian coordinates of the evader in the reduced space are given by:

$$
\begin{aligned}
x &= L \sin \phi \\
y &= L \cos \phi
\end{aligned}
\tag{30}
$$

Assuming that the pursuer does not move, its velocities are given by:

$$
\begin{aligned}
\dot{x} &= v_1 \sin v_2 \\
\dot{y} &= v_1 \cos v_2
\end{aligned}
\tag{31}
$$

Using Eqs. (30) we obtain an expression for $\tan \phi$, and we differentiate this to obtain an expression for $\dot{\phi}_e$, which represents the rate of change of ϕ when the pursuer does not move.

$$
\begin{aligned}
\frac{d}{dt} \tan \phi &= \frac{d}{dt} \frac{x}{y} \\
\dot{\phi}_e \sec^2 \phi &= \frac{y\dot{x} - x\dot{y}}{y^2} \\
\dot{\phi}_e &= \frac{\cos \phi \dot{x} - \sin \phi \dot{y}}{L}
\end{aligned}
\tag{32}
$$

Substituting Eq. (31) in Eq. (32), we obtain

$$
\dot{\phi}_e = \frac{v_1 \sin(v_2 - \phi)}{L}
\tag{33}
$$

The evader's controls that maximize $\dot{\phi}_e$ are $v_1 = V_e^{\max}$ and $v_2 = \phi + \frac{\pi}{2}$ so that

16

$$\dot{\phi_e}^{\max} = \frac{V_e^{\max}}{L} \tag{34}$$

On the other hand, the optimal feedback policy of the pursuer in region R_R dictates that it rotates in place at maximal angular velocity $\omega_{\max}$. From the DDR control model (refer to Eq. (3)), one has that if the DDR pursuer does not translate and it rotates at maximal angular velocity in the direction that makes ϕ decreases as much as possible then

$$\omega^{\max} = \frac{V_p^{\max}}{b} \tag{35}$$

Subtracting this pursuer's maximal angular velocity from $\dot{\phi_e}^{\max}$, one has the resulting $\dot{\phi}$ in the reduced space.

$$\dot{\phi} \le \dot{\phi_e}^{\max} - \omega^{\max} \tag{36}$$

Therefore, one will have that $\dot{\phi} < 0$ if $\dot{\phi_e}^{\max} - \omega^{\max} < 0$, i.e.,

$$\frac{V_p^{\max}}{b} > \frac{V_e^{\max}}{L} \tag{37}$$

but this inequality always holds, since by the definition of this pursuit/evasion problem $V_p^{\max} > V_e^{\max}$, $l \ge b$, and if $L < l$ then the capture occurs. $\qquad\square$

Based on Lemma 4, the proof of Theorem 2 is provided:

Proof. First, if the evader at position (L, ϕ) is in region R_R, with $\phi < \phi_v$, by Lemma 4 $\dot{\phi} < 0$ in this region, so it will eventually falls into R_S. In this case, since the time-optimal feedback policy for the pursuer dictates that it moves in a straight line in R_S, it is possible that $\dot{\phi} > 0$ in this region; however, ϕ never becomes greater than S since to do so, the evader should either move in region R_R having $\dot{\phi_e}^{\max} > \omega^{\max}$ (that is $\dot{\phi} > 0$), which from Lemma 4 is impossible, or cross the barrier surface (BS) which is also impossible (see Ruiz et al. (2013)). This completes the proof. $\qquad\square$

Remark 1: In Theorem 2, both $\phi_0 < S$ or $\phi_0 > S$ are allowed.

Remark 2: The proposed method is able to estimate the correct evader's position on the reduced space of the pursuer, even if the evader rotates, provided that at least seven points of the visual target are visible to the pursuer.

Another sensing issue is that the pattern of points on the evader (visual target), which is used to estimate the state of the evader, can be occluded by the evader's body. Whether or not some (or even all) points on the visual target will be occluded from the pursuer's location by the evader's body depends on the evader's appearance and on the evader's motion over the reduced space (i.e. relative to the pursuer). In this work we assume that enough points for the evader's state estimation (at least 7) belonging to visual target will not be occluded during the game.

However, we consider that it may be feasible to relax this assumption using several visual targets on the evader's body. If the evader can be marked with several visual targets then it is possible to guarantee that at least one visual target is always visible to the pursuer. In many cases, this may be ensured simply by placing copies of this target symmetrically around the center of the evader's body. In this case only two auxiliary images are needed as before at the initialization phase.

Finally, it is interesting to notice that whenever an omnidirectional camera is used and the evader lies outside the set of angles delimited by angle S, the complete state of the evader does not need to be estimated. The bearing measurement of the visual target computed directly in the image can be used to detect this case e.g. by computing the center or mass (or first moment) of the point features. The pursuer must rotate in place at maximal speed to bring the evader within the bound established by angle S. Then, when the evader lies within the bounded field of view the state estimation is performed as explained above.

6.   Simulations

In this section, we present some simulation results of the pursuit-evasion game. We use m/s as units for velocities, meters for distance, and seconds for time. In the realistic space, we will describe trajectories for both the pursuer and the evader over a global reference frame in a Cartesian plane. In the reduced space, we will refer to trajectories of the system, i.e., relative motions of the evader with respect to the pursuer in a local reference frame defined by the pursuer.

First, we show the case in which the pursuer does not use a closed-loop motion policy. Second, we present simulations where the pursuer uses a conventional camera to obtain point features that allow it to estimate the evader's state. Finally, we show simulation where the pursuer uses an omnidirectional camera.

We present five simulation experiments, in all the simulations the parameters were $V_p^{\max} = 1$, $V_e^{\max} = 0.5$, $b = 1$ and $l = 1$. *We have included a video, which is available at the multimedia material of this paper*, showing the simulation results presented in the third (Figs. 10-12(c)), fourth (Figs. 13(a)-15(b)) and fifth (Figs. 16-18(c)) experiments.

6.1   *Open-loop pursuer motion policy*

The two simulations presented in this subsection have as objective to show that it is crucial for the pursuer to use a state feedback-based motion policy in the case of an unpredictable evader. In both simulations the evader is initially located at $(x = 1.08, y = 0)$ in the reduced space.

In the first simulation, we will show an example where both players apply their optimal strategies. The pursuer wins by capturing the evader. The pursuer captures the evader in 3.71 sec.

Fig. 8(a) shows in the realistic space the trajectories of the evader and the pursuer. In Fig. 8(a), P_I and E_I are the initial positions of the pursuer and the evader, and P_F and E_F the positions where capture is attained.

Figure 8(b) shows the system trajectory on the reduced space for the same experiment. In this figure, the initial position of the evader in the reduced spaces is denoted by an I and the final one by an F.

In Fig. 9(a), we can see the trajectories of both players when the evader follows a suboptimal strategy and the pursuer applies the open-loop optimal strategy, i.e., *the pursuer does not use a feedback strategy based on the evader's location*. The same maximal players' speeds and initial configurations, as in Fig. 8(a), were used.

In this case, we can observe that when the DDR uses an open-loop policy, it cannot capture the evader after 3.71 sec., indeed the distance between both players has increased.

Fig. 9(b) shows the system trajectory on the reduced space. Again, the initial position of the evader in the reduced spaces is denoted by an I and the final one by an F.

Below, we present several simulations for omnidirectional and conventional cameras. We do not compare the proposed approach with other feedback-based motion policy, because to our knowledge there is not other feedback-based approach that guarantees to capture the evader in minimal time. Note that a leader-follower control formulation does not guarantee to capture the evader.
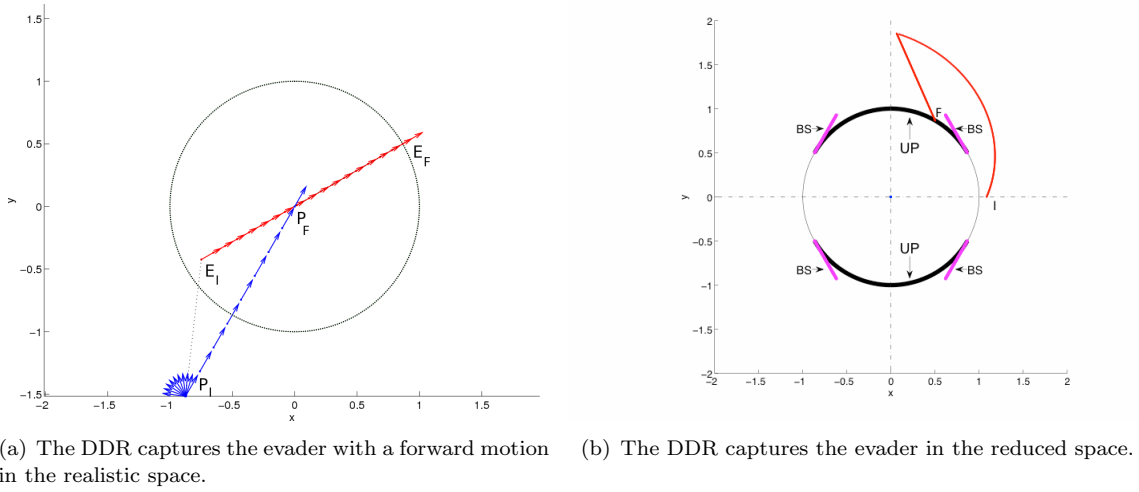
(a) The DDR captures the evader with a forward motion in the realistic space.

(b) The DDR captures the evader in the reduced space.

Figure 8. Open-loop pursuer motion policy and predictable evader

(a) Open-loop pursuer strategy.

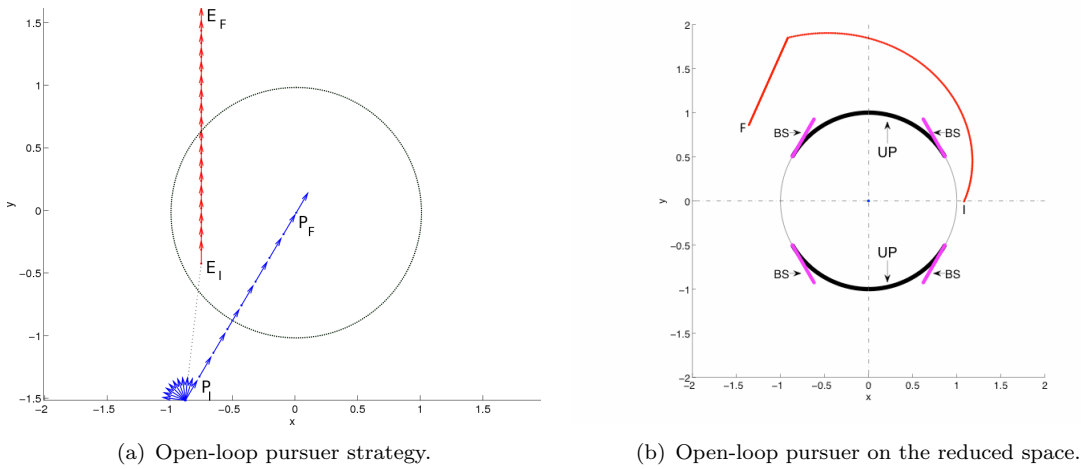(b) Open-loop pursuer on the reduced space.

Figure 9. Open-loop pursuer motion policy and unpredictable evader

6.2   *Conventional Camera*

In this subsection, we present two simulations where the pursuer applies its feedback-based strategy using a conventional camera to estimate the evader's state. In the first one (Figs. 10-12(c)), both the evader and the pursuer follow their time-optimal motion strategies. At the beginning of the game the evader is located at position ($x = 1.07, y = 1.97$) over the reduced space. The time needed to capture the evader is $3.51s$. Fig. 10(a) and Fig. 10(b) show the two auxiliary images taken to the evader before the game starts. Recall that these two images are used to avoid ambiguity about the distance separating the evader and the pursuer during the game. The image shown in Fig. 10(a) was taken from 1 meter to the evader and the image shown in Fig. 10(b) was taken from 2 meters to the evader. In both cases the pursuer's heading points to the evader's center as described in Section 4.

Fig. 11(a) shows the players' trajectories in the realistic space and Fig. 11(b) shows the corresponding trajectory in the reduced space (I indicates the initial evader's state and F the evader's state when the capture is achieved).

Fig. 12(a) shows an image of the pattern used as target at the beginning of the game and Fig. 12(b) shows the image of the target when the pursuer captures the evader. Note that these images are different to the auxiliary images shown in Fig. 10(a) and (b).

Fig. 12(c) shows the trajectories in the image of the 3 vertex points of the target triangular
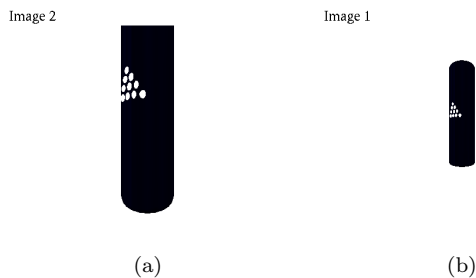
Image 2   Image 1

(a)   (b)

Figure 10. (a) Auxiliary initial image taken to one meter from the evader. (b) Auxiliary initial image taken to two meters from the evader.

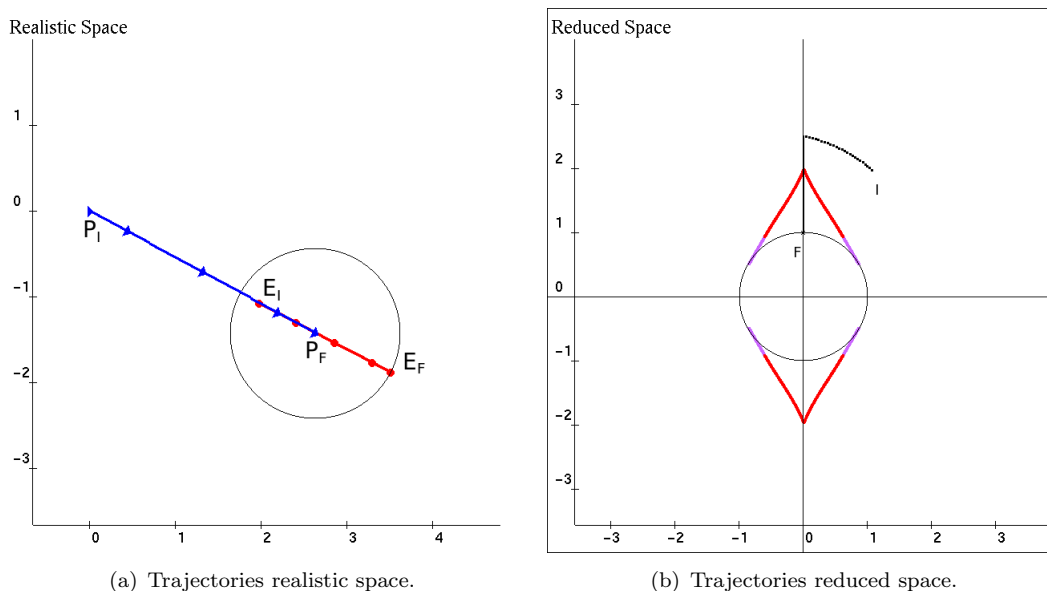(a) Trajectories realistic space.   (b) Trajectories reduced space.

Figure 11. Players' trajectories for a predictable evader

(a) Target image at the beginning of the game
(b) Target image at the end of the game
(c) Points' trajectories in the image of the 3 vertex points of the triangular pattern
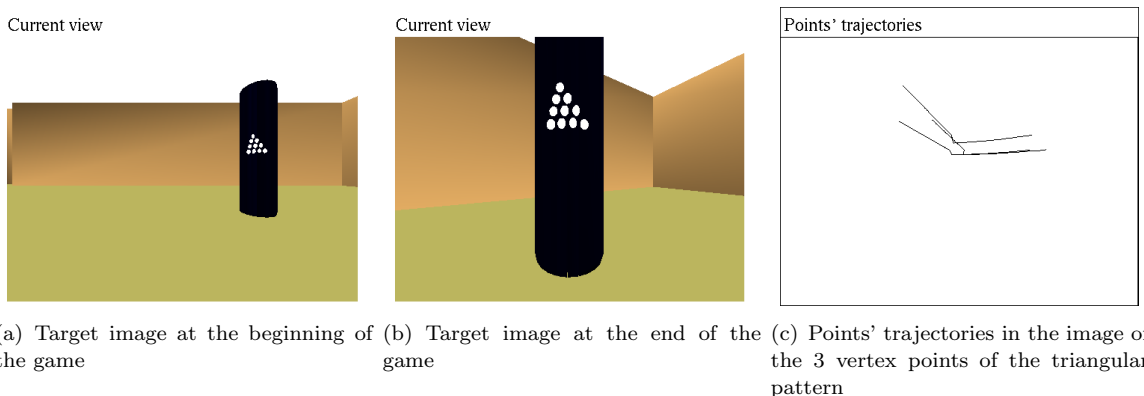
Figure 12. Images from the pursuer's view using a conventional camera

pattern. It can be verified that the points are never located outside the image.

In the second simulation (Figs. 13(a)-15(b)), the evader moves unpredictably (not optimally) and the DDR follows its feedback-based time-optimal motion strategy. At the beginning of the simulation, the evader is located at the same position over the reduced spaced as in the previous simulation, that is $(x = 1.07, y = 1.97)$. The time needed to capture the evader is smaller compared with the simulation in which the evader moves optimally, that is 3.46 sec.

Fig. 13(a) shows the players' trajectories in the realistic space and Fig. 13(b) shows the corresponding trajectories in the reduced space (I indicates the initial evader's state and F the evader's

state when the capture is achieved).

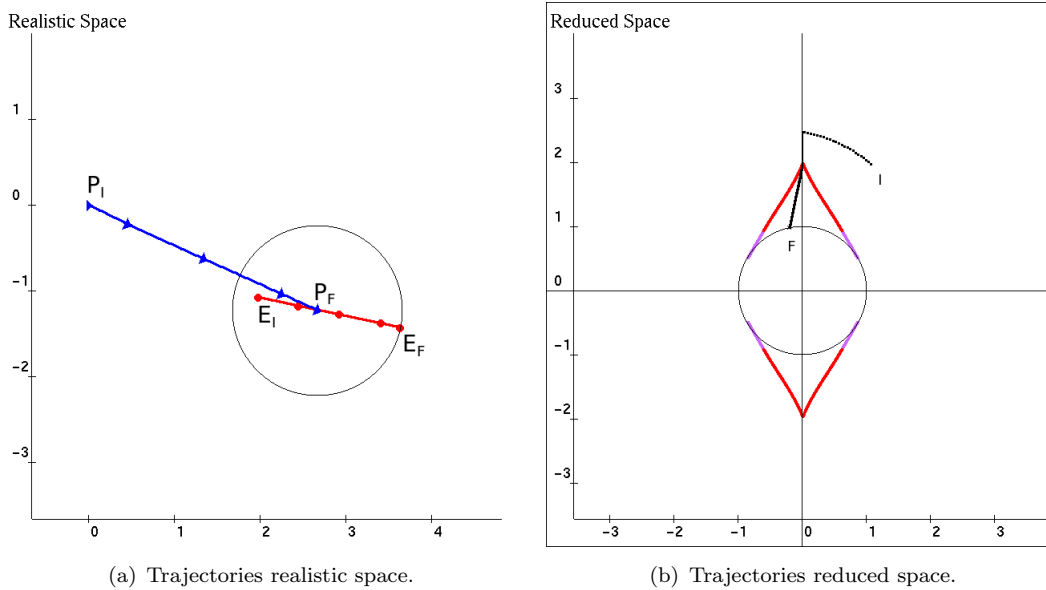(a) Trajectories realistic space.

(b) Trajectories reduced space.

Figure 13. Players' trajectories for an unpredictable evader

Fig. 14(a) shows an image of the target's pattern at the beginning of the game and Fig. 14(b) shows it at the end of the game.
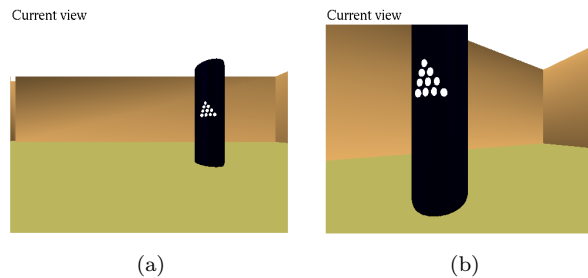

(a)   (b)

Figure 14. (a) Target image at the beginning of the game (b) Target image at the end of the game

A snapshot of the game is shown in Fig. 15(a). The white lines in the image are used to depict the limited field of view of the conventional camera used by the pursuer.

Fig. 15(b) shows the trajectories in the image of the 3 vertex points of the triangular target pattern used as visual target.

6.3 *Omnidirectional Camera*

In the following simulations the pursuer uses an omnidirectional camera to detect the target. An omnidirectional camera provides a field of view of $360°$. The game begins with the target located at $(x = 1.5, y = 0.75)$ in the reduced space. The evader moves unpredictably (not optimally) and the pursuer applies its feedback-based time-optimal motion policy. The time to capture the evader is 3.42 sec.

Fig. 16(a) shows the auxiliary triangular pattern taken to 1 meter from the evader. Fig. 16(b) shows the auxiliary triangular pattern taken to 2 meters from the evader. The center of the evader is aligned with the pursuer heading.

Fig. 17(a) shows the trajectories of the players in the realistic space. Fig. 17(b) shows the trajectory of the evader relative to the pursuer (trajectory of the system in the reduced space).
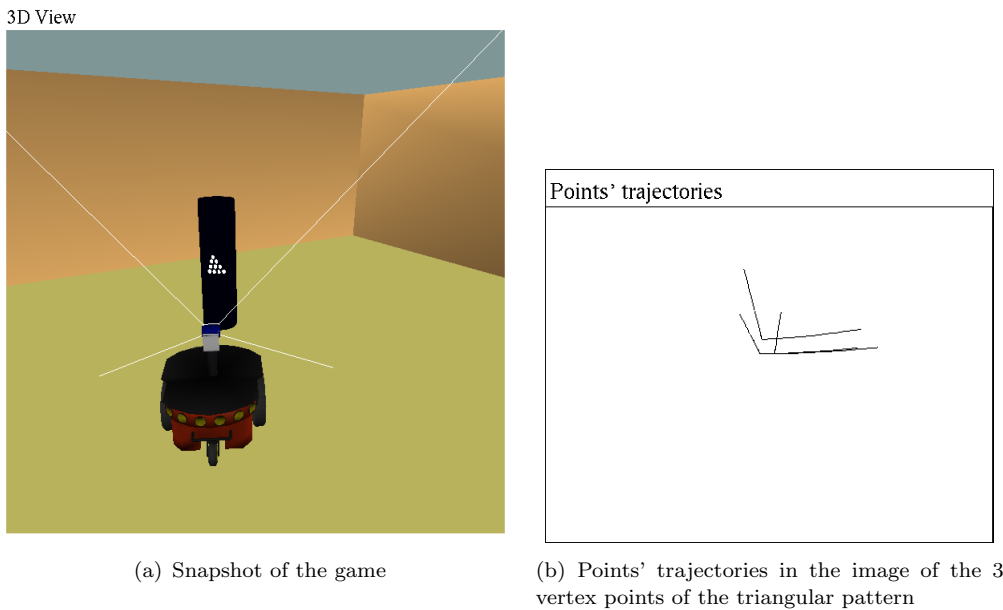
(a) Snapshot of the game

(b) Points' trajectories in the image of the 3 vertex points of the triangular pattern

Figure 15. Snapshot of the game and points' trajectories in the image

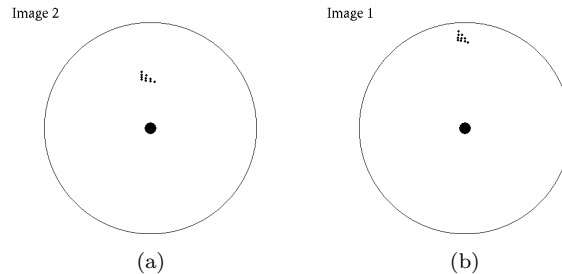(a)   (b)

Figure 16. (a) Auxiliary triangular pattern taken to 1 meter from the evader. (b) Auxiliary triangular pattern taken to 2 meters from the evader.

Fig. 18(a) shows the pattern of points used as visual target at the beginning of the game. Fig. 18(b) shows it at the capture time (end of the game). Fig. 18(c) shows the 3 vertex points' trajectories of the triangular pattern in the omnidirectional image.

7. Conclusions and Future Work

In this paper, we have proposed a state feedback-based motion policy for a DDR, which allows the robot to capture an unpredictable omnidirectional evader in minimum time. A main novelty of this work compared with the classical position-based visual servoing approach is that in our proposed approach, the goal for the robot is not to reach a place where a target image is observed but instead its objective is to bring the evader to a specific locus of points in the reduced space representation of the problem called the usable part.

One contribution of this paper is to provide algebraic equations of the regions' boundaries in terms of the reduced space coordinates. We estimate the state of the evader based on images taken by the pursuer using the 1D trifocal tensor. To capture the evader, the evader location is defined in a local reference frame, which makes necessary a new formulation of the estimation of the evader's state. Furthermore, our approach does not require precise camera calibration and it is valid for different types of central cameras. Finally, we have presented a bound over the pursuer's field of view for conventional cameras. If the evader is initially visible, it will remain inside the camera's view regardless of its motion strategy. This work presents an extension to classical optimal control
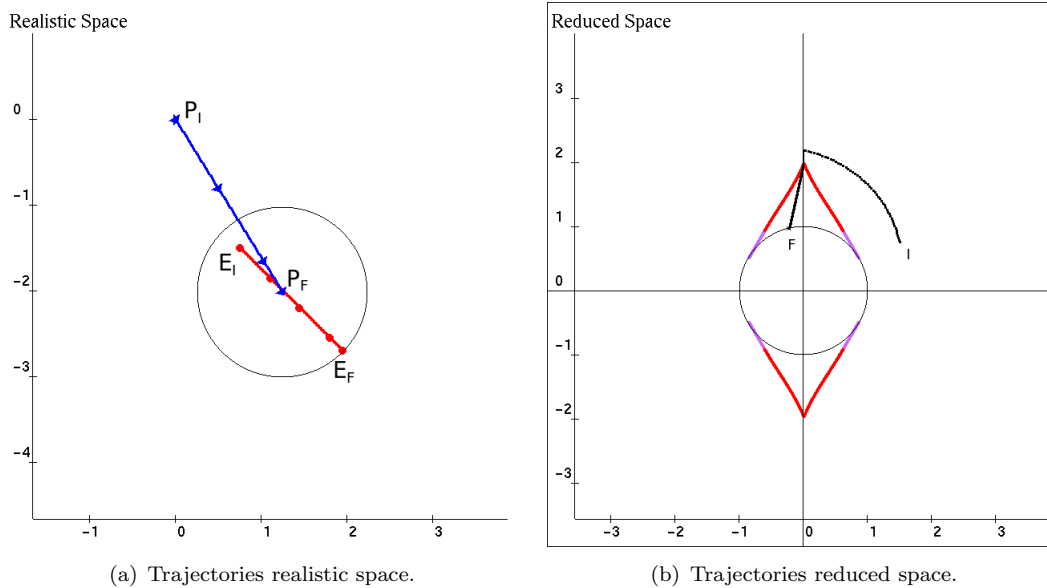
(a) Trajectories realistic space.

(b) Trajectories reduced space.

Figure 17. Players' trajectories for an unpredictable evader

(a) Pattern of points at the beginning of the game

(b) Pattern of points at the end of the game

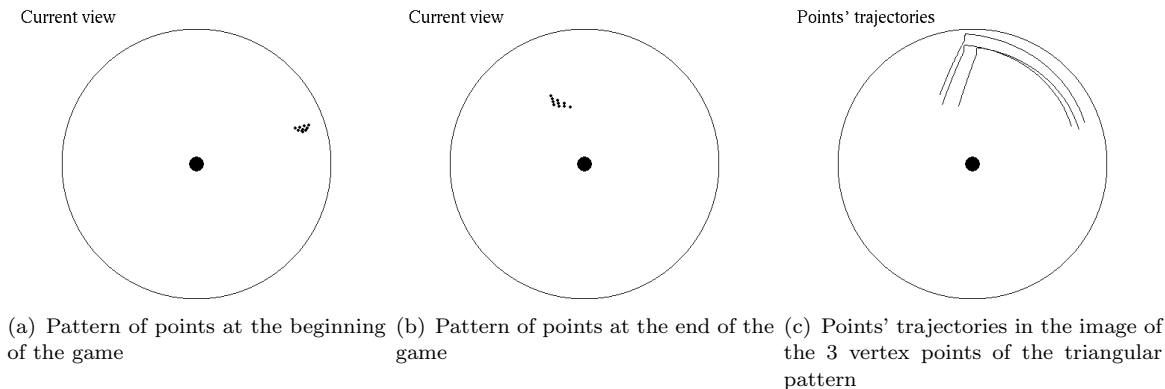(c) Points' trajectories in the image of the 3 vertex points of the triangular pattern

Figure 18. Images from the pursuer's view using an omnidirectional camera

problems by proposing a time-optimal motion policy based on visual feedback.

As future work, we would like to consider the problem of capturing an evader with multiple appearances. We would like to visually estimate the state of the evader without using artificial marks. For this problem, we believe that is feasible to use a set of images which correspond to different views of the evader, finding the one that is most similar to the one observed by the pursuer. In this scheme each visual pattern is related to an evader aspect. Thus, instead of having a pair of auxiliary initial images, a pair of them would be used for each evader aspect to estimate the evader's state. We would also like to explore the problem of generating closed-loop motion policies based on information directly taken from the image space without state estimation. In this paper, it is assumed that the evader moves unpredictably, we would like to address the case in which some information about the evader's motion is known, and to study the effect of this additional information on the time-optimal pursuer motion policy.

References

Balkcom, D.J. & Mason, M.T. (2002). Time Optimal Trajectories for Bounded Velocity Differential Drive Vehicles. *Int. J. Robot. Res.*, *21*(3), 219–232.

Başar, T. & Olsder, G. (1999). *Dynamic Noncooperative Game Theory, 2nd Ed.* SIAM Series in Classics in

Applied Mathematics, Philadelphia.

Bandyopadhyay, T., Ang Jr., M.H. & Hsu, D. (2007). Motion planning for 3-D target tracking among obstacles. *In Proc. Int. Symp. on Robotics Research*, 267–279.

Bhadauria, D. & Isler, V. (2011). Capturing an Evader in a Polygonal Environment with Obstacles. *In Proc. Int. Joint Conf. Artif. Intell.*, *3*, 2054-2059.

Bhattacharya, S. and Hutchinson, S. (2010). On the existence of nash equilibrium for a two player pursuit-evasion game with visibility constraints. *Int. J. Robot. Res.*, *29*(7), 831–839.

Bhattacharya, S. & Hutchinson, S. (2011). A Cell Decomposition Approach to Visibility-Based Pursuit Evasion among Obstacles. *Int. J. Robotic. Res.*, *30*(14), 1709–1727.

Becerra, H.M. & Sagues, C. (2013). Exploiting the Trifocal Tensor in Dynamic Pose Estimation for Visual Control. *IEEE Trans. on Control Syst. Tech.*, *21*(5), 1931–1939.

Chaumette, F. & Hutchinson, S. (2006). Visual servo control. I. Basic approaches. *IEEE Robot. Autom. Mag.*, *13*(4), 82–90.

Chung, T., Hollinger, G. & Isler, V. (2011). Search and pursuit-evasion in mobile robotics: A survey. *Auton. Robot.*, *31*(4), 299–316.

Chung T.H. (2008). On Probabilistic Search Decisions under Searcher Motion Constraints. *In Proc. Int. Workshop Algorithmic Found. Rob.*, 501–516.

Efrat, A., Gonzalez, H.H., Kobourov, S.G. & Palaniappan, L. (2003). Optimal Motion Strategies to Track and Capture a Predictable Target. *In Proc. IEEE Int. Conf. Robot. Autom.*, *3*, 3789–3796.

Faugeras, O., Quan, L., & Strum, P. (2000). Self-Calibration of a 1D Projective Camera and Its Application to the Self-Calibration of a 2D Projective Camera. *IEEE Tran. on Pat. Analysis and Mach. Intell.*, *22*(10), 1179–1185.

Geyer, C. & Daniilidis, K. (2000). An unifying theory for central panoramic systems and practical implications. *In Eur. Conf. on Comp. Vis.*, 445–461.

Guerrero, J.J., Murillo, A.C. & Sagues, C. (2008). Localization and matching using the planar trifocal tensor with bearing-only data. *IEEE Trans. on Robotics*, *24*(2), 494–501.

Guibas, L., Latombe, J.-C., LaValle, S.M., Lin, D. & Motwani, R. (1999). Visibility-based pursuit-evasion in a polygonal environment. *Int. J. Comput. Geom. Appl.*, *9*(5), 471–494.

Hollinger, G., Singh, S., Djugash, J. & Kehagias A. (2009). Efficient Multi-robot Search for a Moving Target. *Int J. Robot. Res.*, *28*(2), 201–219.

Isaacs, R. (1965). *Differential Games.* Wiley, New York.

Isler, V., Kannan, S. & Khanna, S. (2005). Randomized Pursuit-Evasion in a Polygonal Environment. *IEEE Trans. on Robotics*, *5*(21), 864–875.

Jung, B. & Sukhatme, G. (2002). Tracking targets using multiple robots: the effect of environment occlusion. *Auton. Robot.*, *12*, 191–205.

LaValle, S.M., González-Baños, H.H., Becker, C. & Latombe, J.-C. (1997). Motion Strategies for Maintaining Visibility of a Moving Target. *In Proc. IEEE Int. Conf. Robot. Autom.*, *1*, 731–736.

Lopez-Nicolas, G., Gans, N.R., Bhattacharya, S., Sagues, C. & Hutchinson, S. (2010). Homography-Based Control Scheme for Mobile Robots With Nonholonomic and Field-of-View Constraints. *IEEE Trans. on Syst., Man, and Cyb., Part B*, *40*(4), 1115–1127.

Merz, A.W. (1971). The homicidal chauffeur – a differential game. *PhD. Thesis*, Stanford University.

Murrieta-Cid, R., Muppirala, T., Sarmiento, A., Bhattacharya, S. & Hutchinson, S. (2007). Surveillance Strategies for a Pursuer with Finite Sensor Range. *Int. J. Robot. Res.*, *26*(3), 233–253.

O'Kane, J.M. (2008). On the value of ignorance: Balancing tracking and privacy using a two-bit sensor. *In Proc. Int. Workshop Algorithmic Found. Rob*, 235–249.

Parker, L. (2002). Algorithms for Multi-Robot Observation of Multiple Targets. *Auton. Robot.*, *12*, 231-255.

Ruiz, U., Murrieta-Cid, R. & Marroquin, J.L. (2013). Time-Optimal Motion Strategies for Capturing an Omnidirectional Evader Using a Differential Drive Robot. *IEEE Trans. on Robotics*, *29*(5), 1180–1196.

Shi, J. (2014). Relationship between maximum principle and dynamic programming for stochastic differential games of jump diffusions. *Int. Journal of Control*, *87*(4), 693–703.

Soueres, P. & Laumond, J.P. (1996). Shortest paths synthesis for a car-like robot. *IEEE Trans. Autom. Control*, *41*(5), 672–688.

Stump, E., Michael, N., Kumar, V. & Isler, V. (2011). Visibility-Based Deployment of Robot Formations for Communication Maintenance. *IEEE Int. Conf. on Robotics and Automation.*

Tekdas, O., Yang, W. & Isler, V. (2010). Robotic Routers: Algorithms and Implementation. *Int. J. Robot. Res.*, *29*(1), 110–126.

Tovar, B. & LaValle, S.M. (2008). Visibility-based Pursuit - Evasion with Bounded Speed. *Int. J. Robot. Res*, *27*(11-12), 1350–1360.

Vidal, R., Shakernia, O., Jin, H., Hyunchul, D. & Sastry, S. (2002). Probabilistic Pursuit-Evasion Games: Theory, Implementation, and Experimental Evaluation. *IEEE Trans. Robot. Autom.*, *18*(5), 662–669.

Wang, H., Chen, Y. & Soueres, P. (2009). A geometric algorithm to compute time-optimal trajectories for a bidirectional steered robot. *IEEE Trans. on Robotics*, *25*(2), 399–413.

Appendix A. Previous supporting results

In this appendix, we present four lemmas obtained in Ruiz et al. (2013), which are used in this work. For the proofs please refer to Ruiz et al. (2013).

Lemma 5: *The barrier consists of a straight line segment, and it intersects the y-axis in the first quadrant if $\rho_v \geq |\tan S|/\rho_d$ where $S = \cos^{-1}(\rho_v)$ is the angle at the BUP.*

This Lemma implies that for $S = \cos^{-1}(V_e/V_p)$ then $\tau = (b\cos S)/(V_p \sin S)$. See Ruiz et al. (2013) for more details.

Lemma 6: *The DDR switches controls and it starts a rotation in place in the realistic space, at $\tau_s = |\frac{b\cos s}{V_p^{\max} \sin s}|$. If $s \in [0, \pi]$, u_2^* switches first, otherwise u_1^* does.*

Lemma 7: *Let the adjoint equation be:*

$$\frac{d}{dt}\nabla V[\mathbf{x}(t)] = -\frac{\partial}{\partial x}H(\mathbf{x}, \nabla V, u_1^*, u_2^*, v_1^*, v_2^*) \tag{A1}$$

The solution of the adjoint equation (A1) starting at the usable part is

$$V_x = \lambda \sin s, \quad V_y = \lambda \cos s \tag{A2}$$

Lemma 8: *The straight lines trajectories that have an orientation $s \in (\tan^{-1}(\rho_v\rho_d), \cos^{-1}(\rho_v)]$ in the UP of the first quadrant terminate when the DDR switches controls.*